RPE | Radiation Physics & Engineering
A Peer-Reviewed Journal
Published by K.N. Toosi University of Technology
http://rpe.kntu.ac.ir
Research Article

Radiation Physics and Engineering 2027; ?(?):?–?

Radiation dose simulation of a multi-layer gradient shielding structure in low earth orbit using SPENVIS

Zhang Yihan[1,2,*], Liu Miaomiao[a,b], Sun Ruimin[a,b], Yuan Lin[a,b], Wang Boyu[a,b,c,d]

[a] School of Science, Xi'an Polytechnic University, Xi'an 710048, Shaanxi, China
[b] Gansu Nuclear Industry Electromechanical Research Institute, Tianshui 741025, China
[c] Gansu Industrial Vocational and Technical University, Tianshui 741025, China
[d] Xi'an University of Technology, Xi'an 710048, Shaanxi, China

Rejected

HIGHLIGHTS

-
-
-
-

ABSTRACT

In response to the complex space radiation environment faced by low Earth orbit (LEO) spacecraft, this paper conducts a radiation dose simulation study of multi-layer gradient shielding structures using the SPENVIS platform. The AP9/AE9 and CREME96 models were used to calculate the energy spectra of trapped protons, trapped electrons, and galactic cosmic rays, respectively, and the MULASSIS Monte Carlo tool was employed to simulate particle transport and energy deposition processes in multilayer media. With a total surface density fixed at 5 g.cm^{-2}, five shielding structures were designed, including a single-layer aluminum structure, a two-layer Al/PE structure, a three-layer Al/water/PE structure, a three-layer Ta/Al/PE structure, and a five-layer W/PE gradient structure. The simulation results show that low-energy protons are primarily absorbed by the surface material, with little difference in energy deposition among the various configurations; For medium-energy protons , the Ta/Al/PE structure exhibited the lowest total dose, approximately 7% lower than that of a single-layer aluminum structure; for high-energy electrons , the W/PE gradient structure demonstrated the best shielding performance, with a total dose approximately 11% lower than that of a single-layer aluminum structure. This study verifies the comprehensive advantages of multilayer gradient shielding in proton moderation, secondary radiation suppression, and synergistic absorption of electron backscattering, providing a quantitative basis for the design of lightweight radiation protection for near-Earth orbit spacecraft.

KEYWORDS

Space radiation
SPENVIS
Near-Earth orbit
Multilayer gradient shielding
Radiation dose
Lightweight

HISTORY

Received:
Revised:
Accepted:
Published:

1 Introduction

Since the beginning of the 21st century, global space activities have continued to expand, with mission density repeatedly breaking historical records. As space missions grow increasingly complex, protection against high-energy charged particles has become a key factor in the safe operation of spacecraft (Wang et al., 2025). Large-scale low-Earth orbit constellations, such as SpaceX's Starlink and Chinas StarNet, are developing at an accelerated pace, with a single operator now operating thousands of satellites in orbit. At the same time, Chinas space station has achieved long-term crewed habitation, the "Chang'e" and "Tianwen" series of deep-space exploration missions are advancing, and the International Lunar Research Station has entered the feasibility study phase. The spatial scope and temporal duration of human activities in orbit continue to expand, signaling a steady increase in the service life of spacecraft in orbit. Ensuring that spacecraft have longer service lives and higher operational stability has become a critical technological bottleneck that space

*Corresponding author: 240811113@stu.xpu.edu.cn

https://doi.org/

engineering must urgently overcome.

With the rapid development of human spaceflight, satellite constellations, and deep-space exploration technologies, the space radiation environment faced by Low Earth Orbit (LEO) spacecraft is becoming increasingly complex. Major radiation sources include trapped protons and electrons in the Van Allen radiation belts (Earth's radiation belts), galactic cosmic rays (GCRs), and solar particle events (SPEs). These high-energy particles can cause total ionizing dose (TID) effects, single-event effects (SEE), and displacement damage in onboard electronic components, severely affecting the in-orbit lifespan and reliability of satellites (Gutiérrez et al., 2023). Material shielding, as the most mature and widely applied radiation protection method in current engineering practice, is used in the design of various nuclear facilities, medical accelerators, and spacecraft. Although traditional single-layer aluminum shielding solutions are simple to implement, they suffer from low shielding efficiency and high mass penalties. Studies have shown that for a 1,200-km altitude in LEO, the total radiation dose is approximately 10 Krad with 3-mm aluminum (Al) shielding, approximately 45 Krad with 6 mm, and approximately 35 Krad with 9 mm, indicating that the marginal benefit of simply increasing the Al layer thickness diminishes (Jiang et al., 2025). In recent years, multilayer gradient composite structures composed of low-Z hydrogen-rich materials (such as polyethylene and epoxy resin), high-Z absorbing materials (such as tungsten and bismuth), and neutron-absorbing materials (such as boron carbide and boron nitride) have become a research focus. The design of multilayer gradient shielding structures is based on the differing mechanisms by which various radiation particles interact with materials. The core principle involves arranging materials in a gradient order according to their atomic numbers, based on the energy deposition characteristics of each particle in a mixed radiation field. This approach optimizes the attenuation effect for specific particles in each layer while suppressing the generation of secondary radiation, thereby synergistically achieving energy attenuation, secondary radiation suppression, and weight reduction (Anton et al., a). However, due to the broad spatial radiation spectrum, the wide variety of particle types, and the complexity of interaction mechanisms, ground-based experiments struggle to replicate the actual orbital environment. SPENVIS (Space Environment Information System), a standardized space environment simulation platform released by the European Space Agency (ESA), can accurately output particle spectra, radiation doses, and environmental parameters for specified orbits. It is capable of efficiently performing calculations of particle transport and dose deposition through multilayer media and has become the mainstream tool for spacecraft radiation shielding simulation (Daneshvar et al., 2021). Currently, domestic and international research has largely focused on single materials or simple two-layer structures; quantitative comparative studies on gradient structures that combine low-Z and high-Z neutron absorption while balancing shielding efficiency and secondary suppression still require further development (Anton et al., b).

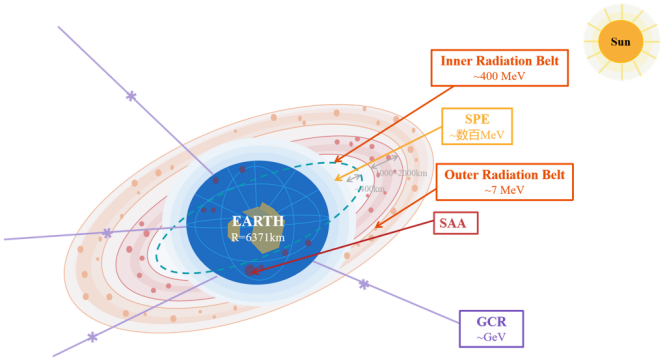


Figure 1: Schematic diagram of the LEO radiation environment.

In summary, since the analysis of space radiation effects is a critical analytical and design process for ensuring the long-term in-orbit service life of spacecraft and the reliability of space missions (**?**), although previous studies have preliminarily confirmed the potential advantages of multilayer gradient shielding structures in mixed radiation fields, systematic simulations and quantitative comparisons of "low-Z-high-Z-neutron absorption" synergistic gradient structures under typical energy spectrum conditions in low Earth orbit remain relatively scarce. Based on the SPENVIS platform, this paper constructed a comprehensive incident energy spectrum covering captured protons, captured electrons, and galactic cosmic rays, designed five shielding structures with constant areal density, and systematically compared the energy deposition characteristics of single-layer, double-layer, triple-layer, and gradient composite structures under different particle types and energy conditions. The study focused on analyzing the mechanisms by which gradient arrangements suppress secondary radiation and enhance shielding efficiency, with the aim of providing simulation support for the design of efficient, lightweight radiation shielding for near-Earth orbit spacecraft.

2 Space Radiation Environment and Shielding Mechanisms

2.1 Characteristics of the Radiation Environment in Low Earth Orbit

Low Earth Orbit (LEO) is the primary operational region for spacecraft such as manned spacecraft, remote sensing satellites, and space stations. The radiation environment in this region consists primarily of the Van Allen radiation belts (Earths radiation belts), galactic cosmic rays (GCRs), and space-borne electron (SPE) events. It is characterized by a broad particle energy spectrum, a wide energy range, and flux variations that are periodic and dependent on orbital parameters and solar activity. This environment is the primary source of Total Ionizing Dose (TID), Space-borne Electromagnetic Effects (SEE), and radiation risks to astronauts. The radiation environment in LEO is shown in Fig. 1. The Van Allen radiation belts are divided into the inner and outer belts. The inner belt consists primarily of high-energy protons,

Uncorrected Proof

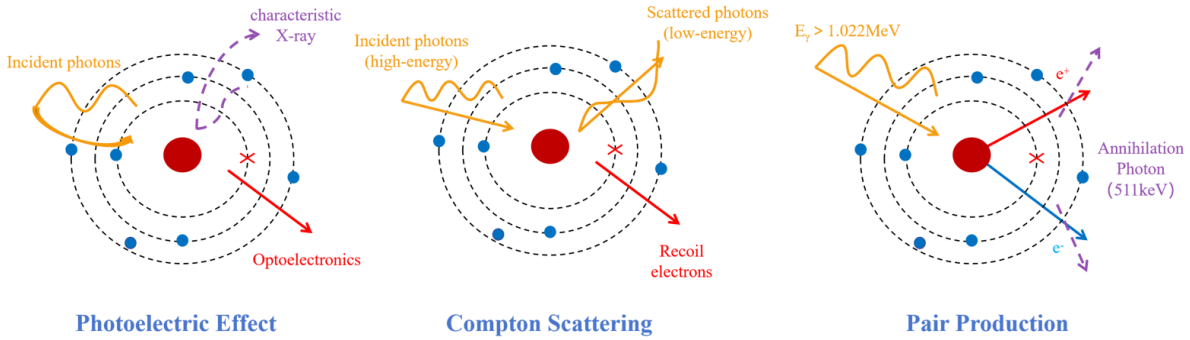


Figure 2: Mechanism of radiation interaction with matter.

with energies ranging from tens of thousands of electron volts to hundreds of megaelectron volts, while the outer belt consists mainly of high-energy electrons, with energies ranging from several megaelectron volts to tens of megaelectron volts. At a typical crewed orbital altitude of approximately 500 km, protons and electrons exhibit stable and relatively high fluxes, serving as the primary sources of continuous cumulative ionizing radiation dose to spacecraft. GCRs originate from high-energy particle fields outside the solar system and consist primarily of protons, alpha particles, and high-energy heavy ions. These particles possess extremely high energies and strong penetrating power, making them difficult to completely block with conventional shielding materials; they are a major factor contributing to deep dose to astronauts and single-event errors (SEEs) in electronic devices. SPE, triggered by solar flares and coronal mass ejections, is characterized by its sudden onset and rapid, short-term surge in flux, posing a severe radiation threat to spacecraft and astronauts in orbit. Studies have shown that orbital inclination significantly alters the radiation environment experienced by spacecraft. For example, in polar orbits with an inclination close to 90°, radiation conditions become exceptionally severe when traversing the North Atlantic Anomaly and regions of open magnetic field lines in the polar regions. Using the AP9/AE9 models in SPENVIS, it is possible to calculate the corresponding particle flux and energy spectrum distribution with reasonable accuracy for specific orbital parameters (Ginet et al., 2013).

2.2 *Mechanisms of Interaction Between Radiation and Matter*

When high-energy particles from space strike a shielding material, they interact with the material through various physical processes, and their intensity decays exponentially according to the Beer-Lambert law (Lei et al., 2026). The interaction mechanisms of different types of particles with matter vary significantly. When high-energy charged particles pass through a medium, they primarily cause ionization and excitation of the materials atoms through Coulomb interactions, resulting in continuous energy deposition; their energy loss behavior can be described by the Bethe-Bloch stopping power (Sigmund and Schinner, 2020). Due to their relatively low mass, electrons are prone to bremsstrahlung in materials with high atomic numbers, producing secondary photons, which in turn increase the radiation dose at the rear end. Protons and heavy ions, with their larger masses and high linear energy transfer values, are prone to triggering nuclear cascade reactions upon interaction with material nuclei, generating secondary radiation components such as secondary neutrons and light nuclei (**?**). Neutral particles such as -rays and photons primarily interact with matter through the photoelectric effect, Compton scattering, and the electron-pair effect. The probability of such interactions is closely related to the atomic number of the material; materials with high atomic numbers have a stronger attenuation capacity for photons but are also more likely to induce secondary radiation (Thomas, 2012). Neutrons are electrically neutral and cannot directly cause ionization; they are primarily moderated through elastic scattering and absorbed via nuclear reactions. Hydrogen-rich materials provide excellent moderation for fast neutrons, while elements such as boron, lithium, and gadolinium have high absorption cross sections for thermal neutrons. Monte Carlo simulations statistically reproduce particle transport processes by randomly sampling the free path and interaction types based on cross sections (Vaquer et al., 2025). The mechanism of interaction between radiation and matter is shown in Fig. 2.

2.3 *Multi-layer Gradient Shielding*

The core design concept of multi-layer gradient shielding is to arrange the material layers in a gradient from low to high atomic number, utilizing the differing responses of materials with different atomic numbers to radiation particles of various types and energies to maximize overall shielding effectiveness. However, in a multi-layer structure, the attenuation mechanisms of each layer differ fundamentally; the attenuation mechanisms of multi-layer structures are shown in Table 1.

Managing secondary radiation is one of the core challenges in multi-layer shielding design. Research has shown that nuclear reactions triggered by the interaction of high-energy particles with shielding materials can produce secondary neutrons and gamma rays. If the shielding design is inadequate, the contribution of this secondary radiation may outweigh the attenuation benefits of primary radiation, causing the total dose at the target location to increase rather than decrease (XUN et al., 2016). Ankit

Uncorrected Proof

Table 1: Attenuation Mechanisms of Multilayer Structures.

Radiation Type	Outer Layer (Low Z) Interaction	Middle Layer (Medium Z) Interaction	Inner Layer (High Z) Interaction
High-energy protons	Coulomb scattering; nuclear fragmentation	Deposition of residual energy	Minimal residual absorption
Captured electrons	Partial energy loss	Primary stopping layer	Absorption of bremsstrahlung
Secondary neutrons	Elastic scattering (thermalization)	Moderate absorption cross section	Capture reactions
Secondary gamma rays	Penetration (low cross section)	Partial Compton scattering	Strong absorption via the photoelectric effect

Gohel et al. found (Gohel and Makwana, 2022) that high-energy electrons can induce bremsstrahlung in high-Z materials; if a high-Z layer is placed on the outer surface directly exposed to the electron environment, a large number of secondary photons will penetrate into the interior. High-energy protons have a large nuclear reaction cross section in high-atomic-number materials and readily produce various secondary particles such as neutrons and pions (Itas et al., 2025); In contrast, while low-Z materials produce less secondary radiation, their ability to attenuate gamma rays is relatively weak (Rode, 2016). Therefore, the rationale behind gradient arrangement is to have low-Z materials first address the "particle radiation" issue-that is, to slow down protons and reduce nuclear reactions-and then utilize high-Z materials to address the "photon radiation" issue-that is, to absorb secondary gamma rays (Arif Sazali et al., 2019). Compared to a simple stacking of a single material, this gradient arrangement allows each layer to attenuate the type of radiation for which it is most effective. Multi-layer shielding designs are typically optimized under the constraint of constant areal density, that is, finding the optimal combination of materials and thickness ratios while keeping the total shielding mass constant. Alizadeh et al. (Alizadeh et al., 2024) used the MCNPX Monte Carlo simulation method to design a three-layer Al-water-polyethylene (PE) shielding structure. Their results showed that the optimized three-layer shielding structure could reduce the shielding mass by 38.88% and 39.69%, respectively, compared to an Al shield of equivalent effectiveness in 10 MeV and 50 MeV proton environments. Guan et al. (Guan et al., 2025) proposed a multi-objective optimization strategy combining uniform design with Monte Carlo simulation, which can simultaneously optimize shielding performance in both proton and electron environments. Fetzer A et al. (Anton et al., c) simulated thousands of multilayer shielding configurations to address the total ionizing dose shielding problem for GTO-orbit nanosatellites and found that configurations with low-Z materials placed on top of high-Z materials resulted in the lowest dose. Compared to an Al shield of equal mass, the optimized PE-Pb bilayer shield reduced the total ionizing dose by 50%.

Research has shown that the core advantage of gradient composite shielding materials (Ahmad et al., 2023) lies in the continuous or quasi-continuous variation of their composition along the thickness direction, which fundamentally eliminates the interlayer thermal stress caused by abrupt changes in the coefficients of thermal expansion between different material layers in traditional multilayer structures. This effectively prevents delamination and debonding failures, resulting in superior structural integrity and long-term durability under the harsh thermal cycling conditions of space. At the same time, this material retains the functional gradient design concept of transitioning from low-Z to high-Z, enabling it to maintain good shielding performance even in mixed radiation fields of high-energy particles and γ-rays. Furthermore, gradient distribution forms-such as linear, exponential, or power-law variations-offer strong design flexibility, allowing the distribution of components within the material along the thickness direction to be adjusted according to the target radiation spectrum, thereby achieving synergistic optimization of shielding and mechanical properties. The gradient composite materials developed by Hu et al. (Hu et al., 2020) for shielding neutrons and gamma rays demonstrate that gradient structures can significantly enhance the mechanical integrity of the material while maintaining shielding effectiveness.

3 SPENVIS Simulation Model

3.1 Introduction to the Simulation Tool

SPENVIS, an online space environment analysis platform developed by the European Space Agency (ESA), integrates orbit definitions, radiation environment models, particle transport tools, and dose calculation methods into a unified web framework, enabling users to complete the entire simulation process-from orbit input to radiation effect assessment-without installing local software (Calders et al., 2018). When modeling the radiation environment of a target orbit using the SPENVIS platform, the next-generation AE9/AP9 models can be employed to calculate the differential energy spectra of captured electrons and protons, respectively. The CREME96 model is selected to calculate the differential energy spectrum of galactic cosmic ray particles, and the calculation results for each component are superimposed to synthesize the comprehensive incident energy spectrum for the orbit. This spectrum covers a broad energy range from keV to GeV and provides a relatively comprehensive representation of the actual radiation environment in near-Earth orbit (Trichtchenko et al., 2014). SPENVIS outputs the calculation results as the distribution of differential flux versus energy, serving as a unified incident source for MULASSIS simulations and

Uncorrected Proof

Table 2: Simulation Parameters for LEO Orbit Satellites.

Parameter	Set Value	Parameter Description
Orbit Type	Sun-synchronous orbit	--
Orbit Altitude	500 km	Typical operational altitude for low Earth orbit missions
Incident Particle Types	Protons, neutrons, electrons	--
Number of Simulated Particles	1E6	--
Incident Energy	10 MeV, 10^2 MeV, 10^3 MeV	Monoenergetic
Angular Distribution	98°	Geostationary orbitTransiting the South Atlantic Anomalous Region (SAA)
Reference Ephemeris	2025.50.03	Aligned with the solar activity cycle to match space environment simulation conditions

ensuring the comparability and consistency of dose assessments under different shielding structures.

MULASSIS is a multi-layer shielding simulation tool integrated with SPENVIS, based on the Geant4 Monte Carlo transport code (Al Zaman and Kunja, 2023). The MULASSIS module employs a one-dimensional flat-plate multi-layer geometric model, in which particles incident perpendicularly (normally) on the shielding structure. It uses the Monte Carlo method to simulate particle transport, interactions, energy deposition, and secondary particle production processes within multi-layer media (Jiggens et al., 2014). The simulated physical processes include electromagnetic and nuclear interactions, covering a complete range of physical mechanisms such as ionization, excitation, scattering, and nuclear reactions. The tool can accurately calculate total ionizing dose, non-ionizing energy loss, particle flux, and depth dose distribution. The simulation outputs the total dose at the rear surface of the shield, the dose deposition curve along the thickness direction, particle flux attenuation results, and the contribution ratio of secondary particles, which are used to systematically evaluate the protective effectiveness of different shielding structures.

To ensure simulation accuracy and computational efficiency, all cases employ uniform physical parameters and convergence criteria; the incident energy spectrum is directly taken from the orbit-averaged results of SPENVIS, and parameters such as the density, composition, and atomic number of the shielding materials are obtained from standard material databases. Using the method of controlled variables, the study examined the effects of material type, areal density, and layer sequence combinations on shielding performance, establishing a correlation between dose and areal density to provide a quantitative basis for the design of lightweight shielding for near-Earth orbit spacecraft.

3.2 Orbit Parameter Settings

This paper conducts radiation environment simulation and analysis using the SPENVIS space environment simulation platform. To comprehensively investigate the impact of solar activity on the orbital radiation environment, the simulation process sets two operating conditions: solar maximum and solar minimum. For the proton and electron particle environment in LEO, industry-standard AP9/AE9 radiation environment models were used for simulation calculations. These models accurately characterize the particle radiation distribution characteristics of the target orbit, ensuring the accuracy and reliability of the simulation data (Johnston et al., 2015). The simulation parameters for LEO satellites are shown in Table 2.

Based on the above orbital parameters, integral flux data for captured particles in this orbital environment were extracted using the AP9/AE9 models in SPENVIS. For an orbit at an altitude of 500 km and an inclination of 98, the average flux of captured electrons with energies greater than 1 MeV is approximately 1.2×10^6 particles.s^{-1}.cm^{-2}, and the average flux of captured protons with energies greater than 10 MeV is approximately 5.8×10^3 particles.s^{-1}.cm^{-2}. These flux levels serve as the environmental input benchmarks for the subsequent MULASSIS one-dimensional flat-plate model.

3.3 Shielding Design Solutions

High-energy charged particles in space, such as protons and electrons, are the primary sources of space radiation that cause irradiation damage to spacecraft, leading to performance degradation and equipment failure. The appropriate selection and development of high-performance radiation shielding materials are key technical approaches to mitigating the hazards of space radiation and ensuring the reliable in-orbit operation of spacecraft. Aluminum (Al) and tantalum (Ta), as the most widely used conventional shielding materials in the aerospace field, each possess distinct advantages and limitations in different radiation scenarios due to their respective characteristics of low atomic number and low cost, versus high density and strong blocking capability. To address the engineering requirement for shielding against high-energy protons in the inner radiation belt, researchers both domestically and internationally have conducted systematic studies based on Monte Carlo simulation methods, focusing on two dimensions: the development of new materials and the optimization of multilayer structures.

Zhang Zhenlong et al.(Zhang et al., 2023) developed a novel composite material and used the Geant4 simulation tool to compare its shielding performance with that of aluminum (Al), tantalum (Ta), and “sandwich” structure materials. The results showed that, for the same shielding mass, compared with aluminum shielding, the novel composite material could reduce the total ionizing dose by 40% and the displacement damage dose by 50%. Transmitted proton counting tests were conducted at ground level us-

Uncorrected Proof

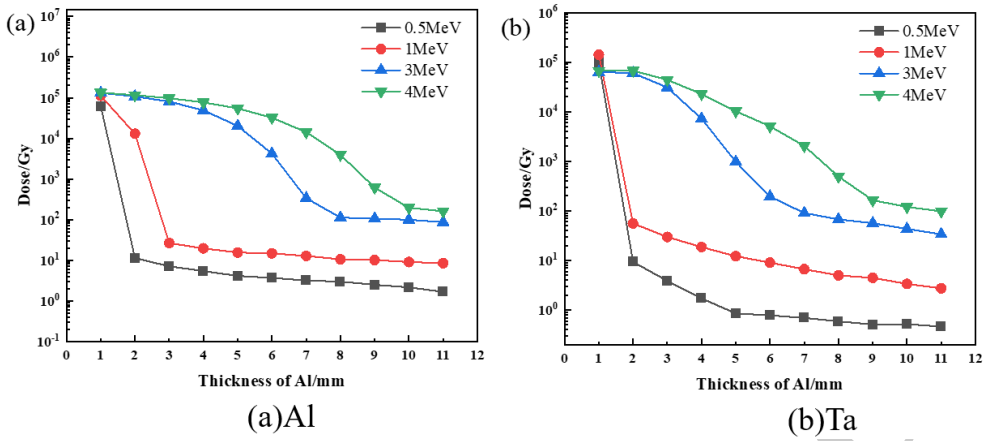


Figure 3: Depth dose distribution curves of Al and Ta (Xiaojun et al., 2007).

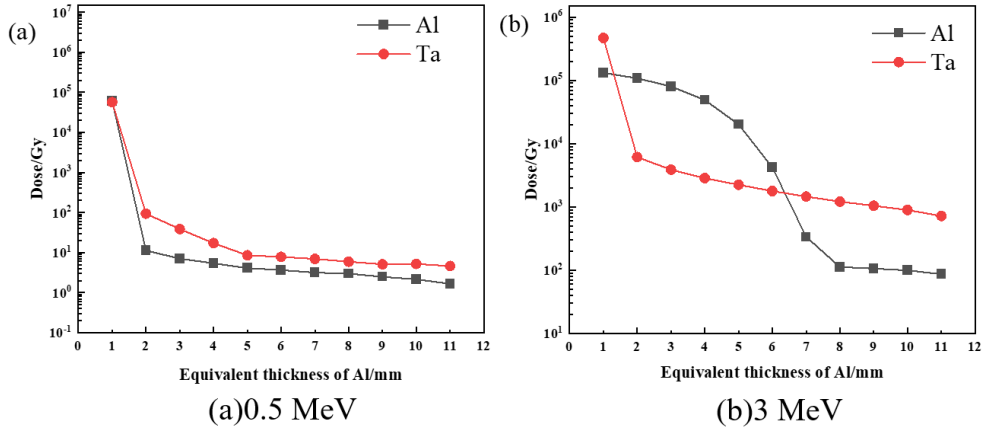


Figure 4: Dosage depth curves of Al and Ta under electron radiation at 0.5 MeV and 3 MeV (Xiaojun et al., 2007).

ing 30-60 MeV proton beams behind aluminum and the new material shields; the experimental results agreed well with the simulation results. Yang Xiaojun et al.(Xiaojun et al., 2007) used the MULASSIS program to simulate the shielding effects of Al and Ta against 0.5-3 MeV electrons and found that the dose-depth curves of the two materials exhibited similar trends, as shown in Fig. 3. In the initial stage, the absorbed dose decreases rapidly with increasing thickness, but the rate of decrease slows after a certain thickness is exceeded. Aluminum has a greater effective range than tantalum, but tantalum results in a higher dose from bremsstrahlung radiation. For 0.5 MeV electrons, under the same areal density conditions, aluminum provides better shielding than tantalum, reflecting the advantage of low-Z materials in electron shielding. Therefore, they selected an electron source of a specific energy to perform simulation calculations of the shielding effectiveness, with the results shown in Fig. 4. It can be seen that in the initial stage of the dose-depth curve, metallic Ta provides better shielding than Al; however, the bremsstrahlung dose produced by Ta is higher than that of Al, resulting in a higher absorbed dose for Ta than for Al in the latter half of the curve.

Cai Yulong et al. (CAI et al., 2023) used the MULASSIS program to compare the comprehensive shielding effectiveness of four materials-PE, polypropylene (PP), Al, and Ta-against protons and electrons for satellite orbits passing through the inner radiation belt. The results are shown in Fig. 5. The study found that, at the same areal density, PP and PE provided the best shielding against protons and electrons, while Ta provided the worst. This is because PE and PP contain similar low-Z elements; at the same areal density, they have a higher electron density, making it easier for protons to undergo inelastic interactions with electrons outside the nucleus along their path of transmission, thereby effectively reducing the protons energy.

Bokaie et al. (Bokaie et al., 2024) used numerical simulation methods to study the range characteristics of high-energy protons and electrons for various shielding materials, as well as the radiation dose response patterns at different substrate thicknesses, and systematically compared the differences in shielding performance among eight shielding materials: Al, PE, SiO_2, Cu, Fe, Ti, W, and Ta. Figures 6-a and 6-b illustrate the relationship between the energy of electrons and protons and the mass range of the materials; the horizontal axes represent electron energy and proton energy, respectively, while the vertical axis represents mass range. Under the same particle energy conditions, the mass range of Ti, Fe, Cu, W, Ta, Al,

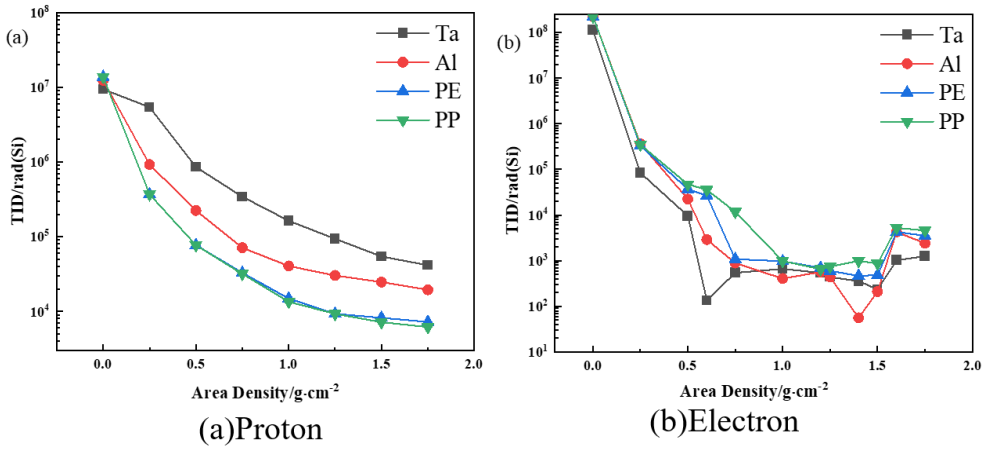


Figure 5: Total dose shielding effect of four different materials under proton and electron radiation (CAI et al., 2023).

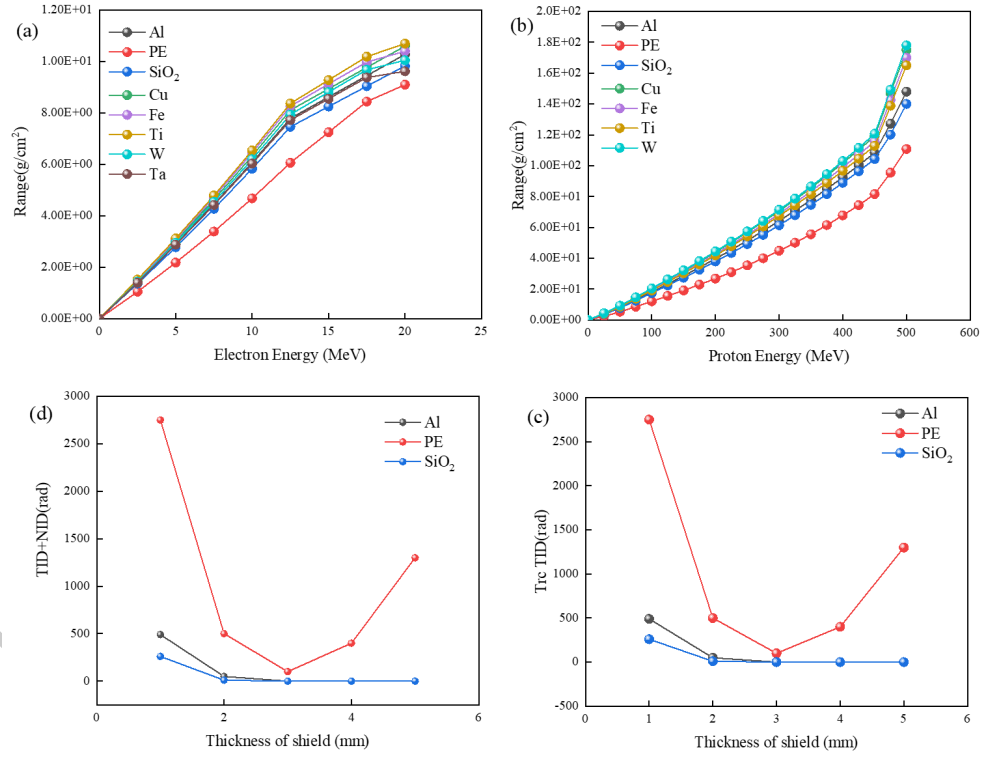


Figure 6: Range characteristics of various shielding materials for high-energy protons and electrons, as well as radiation doses at different thicknesses (Bokaie et al., 2024).

SiO_2, and PE decreases in that order, with PE having the shortest mass range and the strongest particle attenuation capability. Heavy metal materials generally exhibit a higher mass range, and the overall energy range of protons is much greater than that of electrons. Figures 6-c and 6-d illustrate the trends in total ionizing dose (TID) and non-ionizing dose (NID) for Al, PE, and SiO_2 as the substrate thickness varies; For all three materials, the doses exhibit a V-shaped trend as the thickness increases: they first decrease rapidly, bottom out, and then rise slightly. The overall dose values for PE are significantly higher than those for Al and SiO_2, while SiO_2 exhibits the lowest dose in the thick substrate range, with Al falling between the two. The shapes of the two dose curves are highly consistent, with only minor differences in the numerical ranges.

This study employed the MULASSIS software for shielding design. Given that PE possesses excellent proton moderating capabilities, while Al can effectively shield secondary radiation and provide structural strength, this study configured the following five sets of shielding structure specimens, with the total areal density of each set uniformly controlled at 5 $g.cm^{-2}$, as shown in Table 3. Group A served as the single-layer pure aluminum reference; Group B consisted of an Al/PE bilayer structure; Group C comprised an Al/water/PE trilayer structure; Group D utilized a Ta/Al/PE three-layer metal composite, leveraging the high backscattering coefficient of the outer tantalum layer to reflect incident electrons; Group

Table 3: Comparison of different composite shielding structure design schemes.

Group	Structural Type	Materials	Total surface density (g.cm^{-2})	Thickness (mm)		Equivalent aluminum thickness (mm)
A	Single-Layer Reference	Al	5	18.50		18.50
B	Two-Layer Composite	Al/PE	5	9.26 26.60	35.86	18.50
C	Three-Layer Composite	AI/Water/PE	5	5.56 20.00 15.96	41.52	18.50
D	Three-Layer Metal Composite	Ta/Al/PE	5	0.60 7.41 21.28	29.29	18.50
E	Gradient Composite (5 Layers)	80%W+20%PE 60%W+40%PE 40%W+60%PE 20%W+80%PE 0%W+100%PE	5	0.64 0.89 1.35 2.70 10.64	16.22	18.50

E draws on the concept of gradient composites to design a five-layer W/PE gradient structure, in which the volume fraction of W decreases gradually from 80% to 0%. This gradient design features a smooth transition, effectively preventing delamination and cracking of multilayer materials caused by differences in thermal expansion coefficients during thermal cycling.

Based on the surface density calculation Eq. (1), the corresponding thicknesses for the five groups of materials can be determined, as shown in Table 3.

$$\sigma = \frac{m}{s} \tag{1}$$

Here, σ is the surface density of the material, in g.cm^{-2}; m is the mass of the material, in g; and S is the surface area of the material, in cm^2.

It should be noted that, in order to eliminate the superposition effects of complex energy spectra and quantitatively compare the intrinsic shielding capabilities of various materials, the MULASSIS simulations in this section and Section 4 did not directly use the continuous broad energy spectrum described in Section 3.2, but instead adopted the assumption of single-energy particle sources. The simulations were configured with single-energy proton, neutron, and electron sources, with the energy points strictly set at 10^1 MeV, 10^2 MeV, and 10^3 MeV, respectively. This assumption of single-energy cosmic particles facilitates the isolated analysis of the physical interaction mechanisms of materials across different energy ranges, such as total absorption in the low-energy range and secondary radiation from nuclear reactions in the high-energy range.

4 Simulation Results and Analysis

4.1 Analysis of Shielding Performance

To ensure consistency with the units used in relevant domestic and international research literature, this study employed the MULASSIS software to perform particle transport simulations on five shielding structures, all of which had a total surface density of 5 g.cm^{-2}. The simulations employed monenergetic protons, neutrons, and electrons as incident particle sources, with energy points set at 10^1 MeV, 10^2 MeV, and 10^3 MeV, respectively. The particle incidence direction was isotropic, and the number of primary particles per simulation was 1E6. Relative dose was used as the evaluation metric for shielding performance; the simulation results are shown in Fig. 7. As shown in Fig. 7-a, under low-energy 10^1 MeV protons, the energy deposition doses for the five material groups were similar. This is because low-energy protons have a short range and are completely absorbed by the first layer, failing to penetrate into subsequent layers. As the energy increased to 10^2 MeV and 10^3 MeV, the protons' penetration capability significantly increased, and performance differences among the groups began to emerge. Under high-energy proton irradiation at 10^3 MeV, significant differences were observed among the material groups, indicating that placing high-Z materials in the outer layer can effectively dissipate the energy of high-energy protons; Figure 7-b shows that the Al layer has the lowest deposited dose; however, this is because Al has a small neutron scattering cross section, allowing neutrons to penetrate without depositing energy, resulting in limited energy deposition. Effective neutron shielding materials gradually deposit neutron energy within the material through elastic scattering, resulting in higher deposited doses. Consequently, the materials in Group D-with a thicker inner PE layer providing ample neutron moderation pathways-allow the outer Ta layer and the intermediate Al layer to assist in dissipating part of the high-energy neutrons' energy; As shown in Fig. 7-c, under low-energy electrons of 10^1 MeV, the combination of high-Z materials offers significant advantages; however, as electron energy increases, relying solely on high-Z materials makes it difficult to achieve effective shielding. This is because electron shielding requires a balance between the backscattering effect of high-Z materials-which reflects incident electrons back into space-and the absorption of secondary bremsstrahlung radiation by low-Z materials. Group E materials possess high effective atomic numbers and densities, enabling them to effectively backscatter and absorb high-energy electrons, thereby reducing the number of electrons penetrating to the inner layers. Furthermore, as the W content decreases layer

Uncorrected Proof

by layer and the PE content increases, a smooth transition from "high-Z-dominated" to "low-Z-dominated" is achieved, with the innermost PE layer efficiently absorbing secondary X-rays and γ-rays. At the same time, the continuous variation in composition eliminates interlayer interfaces, preventing the reflection and accumulation of secondary radiation at these interfaces.

Figure 8 shows the total ionizing dose for the three types of particles in the five material groups at 10^1 MeV, 10^2 MeV, and 10^3 MeV. For proton irradiation, the total dose for all five groups was approximately 2.50 MeV at 101 MeV, with no significant differences, indicating that low-energy protons are completely absorbed by the surface layer of the materials. At 10^2 MeV, Group D had the lowest total dose at approximately 16.08 MeV, which was about 7% higher than Group A but 8% to 11% lower than Groups B, C, and E; at 1 GeV, Group A had the lowest dose, while Group D's dose was 8% to 11% lower than that of Groups B and C. For neutron irradiation, Groups B, C, D, and E-which contained P or water layers-performed better than Group A at both 10^1 MeV and 10^2 MeV. Among these, Groups D and E had the lowest total doses at 10^1 MeV, demonstrating the effective moderating and absorbing effects of low-Z materials on neutrons. For electron irradiation, there were no significant differences among the groups at 10^1-10^2 MeV; at 10^3 MeV high-energy electrons, Group E performed best, showing a reduction of approximately 11% compared to Group A, indicating that the gradient structure provides synergistic shielding advantages against high-energy electrons. Overall, Group D has a clear advantage in proton and neutron shielding, while Group E stands out in high-energy electron shielding.

Under conditions of equal mass, where the total areal density is 5 g.cm^{-2}, the weight of the shielding material can be described by Eq. (2):

$$\sigma = \sum_{i=1}^{n} \rho_i . t_i = 5 \text{ g.cm}^{-2} \tag{2}$$

where σ is the total areal density, ρ_i is the density of the i-th layer of material, and t_i is the thickness of the i-th layer of material. This formulation ensures that the weight cost of the five shielding structures is exactly the same; therefore, the key criterion for evaluating their relative performance lies in their TID reduction capability per unit weight. Accordingly, the specific dose reduction rate η is introduced as an evaluation metric for the weight-to-efficacy ratio, as shown in Eq. (3) -that is, the percentage reduction in TID for the composite structure compared to the single-layer aluminum reference group at the same weight cost.

$$\eta = \frac{TID_{Al} - TID_i}{TID_{Al}} . \frac{1}{\sigma} . 100\% \tag{3}$$

Here, η is the dose reduction efficiency normalized by surface density, with units of %/g.cm^{-2}; TIDAl is the absorbed dose of the single-layer aluminum reference group, with units of krad; and TIDi is the absorbed dose of the i-th shielding structure, with units of krad.

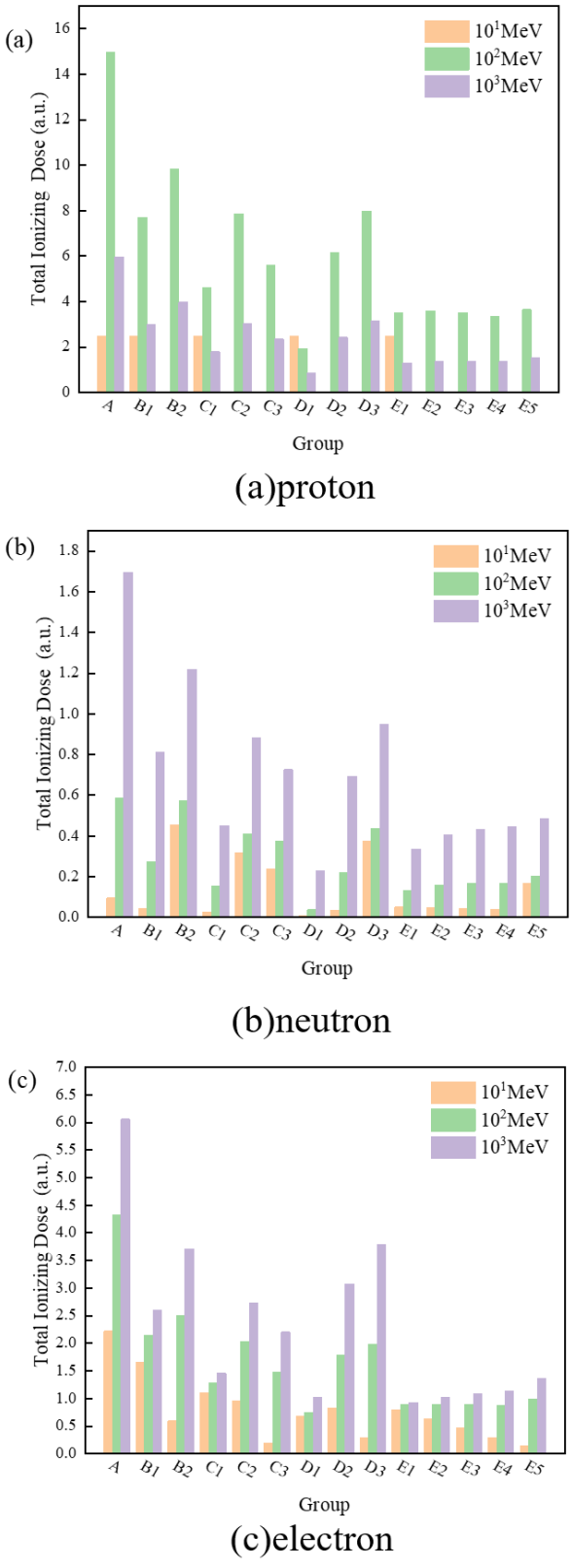


Figure 7: Energy deposition of proton, neutron, and electron sources for the five material groups at energy levels of 10^1 MeV, 10^2 MeV, and 10^3 MeV.

According to the simulation results in Fig. 8, under 10^2 MeV medium-energy proton irradiation, Group D exhibited the lowest TID, with a relative dose reduction efficiency η approximately 7% higher than that of the single-layer Al reference group. In a high-energy electron en-

Uncorrected Proof

vironment, Group E demonstrated the optimal shielding performance, with a TID approximately 11% lower than that of Group A. In terms of the weight-to-efficacy ratio, Groups D and E achieved optimal dose attenuation efficiency in medium-energy proton and high-energy electron environments, respectively, at the same mass cost of 5 g.cm^{-2}. This indicates that, compared to the law of diminishing marginal returns associated with simply increasing aluminum thickness, multilayer gradient structures achieve higher radiation shielding benefits at the same mass cost, highlighting the advantages of lightweight design.

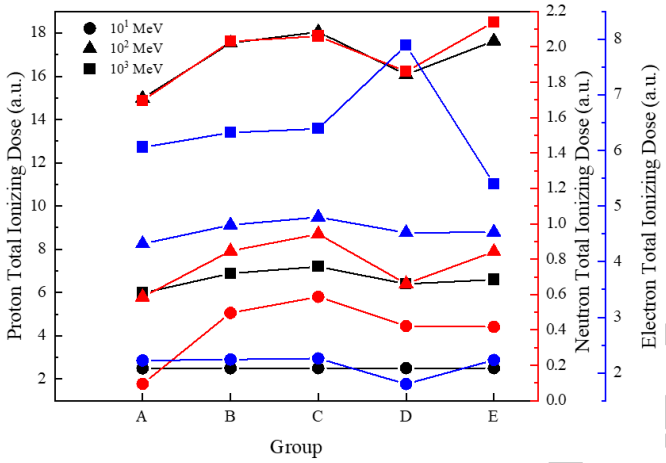


Figure 8: Trends in Total Ionizing Dose for Three Types of Particles at 10^1 MeV, 10^2 MeV, 10^3 MeV.

4.2 Thermodynamics and Damage Mechanisms

In practical space applications, thermodynamic behavior is critical to the long-term reliability of shielding materials, particularly for hydrogen-rich polyethylene (PE) materials. The coefficient of thermal expansion of PE is significantly higher than that of high-Z metals such as aluminum (Al), tantalum (Ta), and tungsten (W). Under the severe thermal cycling conditions of near-Earth orbit-such as when entering and exiting the Earth's shadow-traditional multilayer tiled structures, as represented by Groups B, C, and D, are highly susceptible to enormous thermal stresses caused by abrupt changes in the coefficient of thermal expansion between layers, which can lead to delamination, debonding, or cracking failure. In contrast, the W/PE five-layer gradient structure designed in this paper utilizes a smooth transition in the volume fraction of W along the thickness direction, fundamentally eliminating distinct physical interlayer interfaces. This functionally graded design not only effectively alleviates thermal stress concentration and maintains structural integrity but also prevents the reflection and accumulation of secondary radiation at heterogeneous interfaces, demonstrating superior durability compared to traditional multilayer structures under the harsh thermodynamic conditions of space.

In addition to thermodynamic failure, material damage caused by space particle irradiation is also a key factor determining the service life of shielding layers. The mechanisms of action of different particles determine the patterns of material damage evolution. For protons, high-energy protons can undergo nuclear cascade reactions with the target nucleus, inducing dislocation damage through non-ionizing energy loss, which leads to semiconductor lattice defects; Ta and Al in Group D have higher densities and can effectively block high-energy protons, but this process carries the potential risk of secondary neutron generation. For electrons, the high-Z layers in Group E can attenuate incident electrons through the backscattering effect; however, sustained bombardment by high-energy electrons can trigger hard radiation, generating secondary X-ray and gamma photons; The cumulative effects of long-term irradiation will cause radiation cross-linking or molecular chain degradation in the PE matrix, thereby reducing the materials mechanical properties. Therefore, in addition to minimizing TID, a multi-layer gradient shielding design must comprehensively balance the electron backscattering advantages of high-Z materials against the irradiation aging risks of the low-Z matrix, taking into account both shielding performance and the materials long-term service stability to achieve a synergistic balance between shielding effectiveness and irradiation lifetime.

5 Conclusions

Based on the SPENVIS platform, this paper presents a simulation study of particle transport and energy deposition for five shielding structures under typical near-Earth orbit radiation conditions at a surface density of 5 g.cm^{-2}. It systematically analyzes the single-layer Al, Al/PE bilayer, Al/water/ PE, Ta/Al/PE, and W/PE five-layer gradient structures under three particle types-protons, neutrons, and electrons-at three energy levels: 10^1 MeV, 10^2 MeV, and 10^3 MeV. The main conclusions are as follows:

1. Regarding proton shielding, under low-energy proton irradiation at 10 MeV, all structures completely retained the particles at the surface layer, with similar total energy deposition and no significant differences. At 10^2 MeV, the Ta/Al/PE three-layer structure exhibited the lowest total dose, approximately 7% lower than that of a single-layer aluminum structure; whereas at 10^3 MeV, the single-layer aluminum structure had the lowest total dose, but the Ta/Al/PE structure still outperformed two- and three-layer structures lacking a high-Z outer layer, indicating that the high-Z outer layer plays a positive role in dissipating the energy of high-energy protons.

2. Regarding neutron shielding, composite structures containing polyethylene or water layers outperformed the pure aluminum group at both 10^1 MeV and 10^2 MeV, with the Ta/Al/PE and W/PE gradient structures performing best, verifying the effective moderating and absorption capabilities of hydrogen-rich materials for fast neutrons. Regarding high-energy electron shielding, the W/PE five-layer gradient structure reduced the total dose by

Uncorrected Proof

approximately 11% compared to a single layer of aluminum, significantly outperforming other structures. Its composition transitions smoothly from high-Z to low-Z, achieving a synergistic effect between electron backscattering and the absorption of secondary hard radiation, while simultaneously eliminating interlayer interfaces, which helps suppress the accumulation of secondary radiation.

3. Overall, under the constraint of equal surface density, the Ta/Al/PE structure exhibits superior comprehensive performance in proton and neutron shielding, while the W/PE gradient structure demonstrates distinct advantages in high-energy electron shielding. From the perspective of weight reduction and weight-to-performance ratio, gradient structures offer higher shielding efficiency per unit mass compared to traditional single-layer aluminum; at the same time, the gradient design effectively eliminates interfaces with abrupt thermal stress changes between layers, ensuring the structural reliability of low-Z materials such as PE under in-orbit thermal cycling conditions. By incorporating the mechanisms of proton displacement damage, neutron damage, and γ-radiation damage, multilayer gradient shielding structures-through the rational arrangement of low-Z, medium-Z, and high-Z materials-can effectively address the energy deposition requirements of different particle types and the need for secondary radiation suppression in mixed radiation fields. This represents a key technical approach for enhancing the radiation protection efficiency of near-Earth orbit spacecraft and achieving lightweight designs.

In summary, by rationally arranging low-Z, medium-Z, and high-Z materials, multilayer gradient shielding structures can effectively meet the energy deposition and secondary suppression requirements for different types of particles in mixed radiation fields, representing a key technical approach for enhancing the radiation protection efficiency of near-Earth orbit spacecraft. Future research may further integrate dynamic energy spectra of solar particle events, three-dimensional geometric modeling, and mechanothermal coupling analysis to advance the engineering application of gradient shielding materials.

Acknowledgements

Technical support was provided by the Shaanxi Provincial University Youth Innovation Team for Nuclear Military Ray Flexible Protection Technology, the University Engineering Research Center for Ray Flexible Protection Technology of Shaanxi Province, and the Xi'an Key Laboratory of Nuclear Protection Textile Equipment Technology.

Conflict of Interest

The authors declare no potential conflict of interest regarding the publication of this work.

Funding

The authors declare that no funds, grants, or other financial support were received during the preparation of this manuscript.

References

Ahmad, S., Chang, B., Lian, C., et al. (2023). Design and development study of gradient composite shielding material for nuclear radiation. *Nuclear Engineering and Design*, 414:112517.

Al Zaman, M. A. and Kunja, L. A. (2023). Effectiveness of radiation shields constructed from Martian regolith and different polymers for human habitat on Mars using MULASSIS/GEANT4 and OLTARIS. *AIP Advances*, 13(8).

Alizadeh, A., Rastegarzadeh, G., et al. (2024). Simulation and Design of Optimized Three-Layer Radiation Shielding to Protect Electronic Boards of Satellite Revolving in Geostationary Earth Orbit (GEO) Orbit against Proton Beams. *Journal of Astronomy and Space Sciences*, 41(1):17–23.

Anton, F., Marius, A., Philipp, O., et al. Total ionising dose multilayer shielding optimisation for nanosatellites on geostationary transfer orbit.

Anton, F., Marius, A., Philipp, O., et al. Total ionising dose multilayer shielding optimisation for nanosatellites on geostationary transfer orbit.

Anton, F., Marius, A., Philipp, O., et al. Total ionising dose multilayer shielding optimisation for nanosatellites on geostationary transfer orbit.

Arif Sazali, M., Alang Md Rashid, N. K., and Hamzah, K. (2019). A review on multilayer radiation shielding. In *IOP Conference Series: Materials Science and Engineering*, volume 555, page 012008. IOP Publishing.

Bokaie, Z., Daneshvar, H., Feghhi, S. A. H., et al. (2024). Investigation and Comparison of Materials Using in Radiation Protection of Commercial Parts in LEO Satellite Mission using SPENVIS Software.

CAI, Y., CUI, S., LIU, Y., et al. (2023). Passive shielding against proton and electron in the inner radiation belt. *Nuclear Techniques*, 46(2).

Calders, S., Messios, N., Botek, E., et al. (2018). Modeling the space environment and its effects on spacecraft and astronauts using SPENVIS. In *2018 SpaceOps Conference*, page 2598.

Daneshvar, H., Milan, K. G., Sadr, A., et al. (2021). Multilayer radiation shield for satellite electronic components protection. *Scientific Reports*, 11(1):20657.

Ginet, G., OBrien, T., Huston, S., et al. (2013). AE9, AP9 and SPM: New models for specifying the trapped energetic particle and space plasma environment. *Space Science Reviews*, 179(1):579–615.

Gohel, A. and Makwana, R. (2022). Multi-layered shielding materials for high energy space radiation. *Radiation Physics and Chemistry*, 197:110131.

Uncorrected Proof

Guan, S., Fu, G., Wan, B., et al. (2025). Uniform design for the multi-layer space radiation shielding optimization. *The European Physical Journal Plus*, 140(8):753.

Gutiérrez, O., Prieto, M., Perales-Eceiza, A., et al. (2023). Toward the use of electronic commercial off-the-shelf devices in space: Assessment of the true radiation environment in low earth orbit (LEO). *Electronics*, 12(19):4058.

Hu, G., Shi, G., Hu, H., et al. (2020). Development of gradient composite shielding material for shielding neutrons and gamma rays. *Nuclear Engineering and Technology*, 52(10):2387–2393.

Itas, Y. S., Khandaker, M. U., Hassan, R. A., et al. (2025). Investigations on transition metals (Zn, Co) and alkali metals (Ca, Na) boro-tellurite glasses for gamma ray sensing applications: Physical properties and gamma ray attenuation aspects. *Radiation Physics and Chemistry*, 232:112616.

Jiang, H., Deng, L., and Shi, X. (2025). Simulation of space radiation for polar-orbit spacecrafts at altitude of about 1200 km. In *Journal of Physics: Conference Series*, volume 2965, page 012018. IOP Publishing.

Jiggens, P., Chavy-Macdonald, M.-A., Santin, G., et al. (2014). The magnitude and effects of extreme solar particle events. *Journal of Space Weather and Space Climate*, 4:A20.

Johnston, W. R., O'Brien, T. P., and Ginet, G. P. (2015). Release of AE9/AP9/SPM radiation belt and space plasma model version 1.20. 002. *Space Weather*, 13(6):368–368.

Lei, Y., Xu, P., Lu, C., et al. (2026). Study on Geometric Scattering Effects Correction for Precise Estimation of Fast Neutron Shielding in Polyethylene Materials. *Applied Sciences*, 16(3):1345.

Rode, M. (2016). Interaction studies and Gamma-Ray properties of some low-Z materials. *Nuclear Technology and Radiation Protection*.

Sigmund, P. and Schinner, A. (2020). The bloch correction, key to heavy-ion stopping. *Journal of Applied Physics*, 128(10).

Thomas, D. J. (2012). ICRU report 85: fundamental quantities and units for ionizing radiation.

Trichtchenko, L. D., Nikitina, L., Trishchenko, A., et al. (2014). Highly elliptical orbits for arctic observations: Assessment of ionizing radiation. *Advances in Space Research*, 54(11):2398–2414.

Vaquer, P. A., Rising, M. E., Kulesza, J. A., et al. (2025). Derivation and verification of the direct-sampling method for simulating Monte Carlo flight paths in tetrahedral meshes with linear finite-element cross sections. *European Physical Journal N (Nuclear Science & Technologies)*, 11.

Wang, M., Wang, Q., Xiao, Y., et al. (2025). Review of passive shielding materials for high-energy charged particles in Earth's orbit. *Materials*, 18(11):2558.

Xiaojun, Y., Bo, F., Zhimin, Y., et al. (2007). Radiation shielding effects simulation of multi-layered metal sheets for high energy electrons-applications of MULASSIS software. *Chin. J. Rare Metals*, 31(4):481–485.

XUN, M., HE, C., LU, W., et al. (2016). Secondary particle simulation analysis of high-energy Fe-56 ion inject various shielding material. *Nuclear Techniques*, 39(6):28–34.

Zhang, Z., Liu, Y., Liu, J., et al. (2023). Study on radiation shielding of inner radiation belt protons. *IEEE Transactions on Nuclear Science*, 70(4):701–706.

Uncorrected Proof

©2027 by the journal.

RPE is licensed under a Creative Commons Attribution-NonCommercial 4.0 International License (CC BY-NC 4.0).





To cite this article:

Z. Yihan, L. Miaomiao, S. Ruimin,Y. Lin, W. Boyu. Radiation dose simulation of a multi-layer gradient shielding structure in low earth orbit using SPENVIS. *Radiation Physics and Engineering*, In Press.

DOI:

To link to this article: